Moving MAMMOTH: Stable Motion for a Reconfigurable Wheel-On-Leg Rover

William Reid, Ali Haydar Göktoğan and Salah Sukkarieh
Australian Centre for Field Robotics, The University of Sydney, Australia
[w.reid, a.goktogan, s.sukkarieh]@acfr.usyd.edu.au

Abstract

Reconfigurable wheel-on-leg rovers allow for a variety of locomotion modes and possible instability as a result of configuration changes. Presented is a kinematic model for the actuation of a wheel-on-leg platform along with a tip-over stability model. The kinematic model allows for the superposition of the rover's basic motion primitives, thereby allowing for synchronous motion execution. The stability model allows the operator to observe if the rover is approaching an unstable state. Experimental results using the MAMMOTH (Mars Analogue Multi MOde Traverse Hybrid) rover are presented, and highlight how the kinematic and stability models are utilised to both operate and ensure the safety of the system.

Figure 1: The MAMMOTH (Mars Analogue Multi-MOde Traverse Hybrid) rover.

1 Introduction

Wheel-on-leg rovers are a unique type of exploration platform in that they can drive over benign terrain in an energy efficient manner, while they can also clamber or walk over rugged terrain. Their ability to change pose is also advantageous when wanting to optimize wheel traction, keep specific body orientations and retain stability on rough terrain. However, this high mobility results in motion control complexity. This paper develops a motion model that allows for tele-operated and semi-autonomous operations that take advantage of the rover's reconfigurability and in turn increases the system's terrain exploration capabilities.

The first step in understanding the mobility of any mobile platform is to develop a kinematic model that relates the commanded actuator rates and positions to the overall motion of the platform. Given the large degrees of actuated freedom present in wheel-on-leg platforms, the manner in which each of the actuators should move to achieve a desired full body motion is non-trivial. The kinematic model presented takes basic motion primitives of a wheel-on-leg rover and superimposes them to describe more complex motions that are necessary for full-body pose reconfiguration. For simplicity, operations on a flat surface are assumed. This assumption is the foundation for more complex terrain interaction as part of future research.

Previous kinematic models of highly articulated rovers include the slip, navigation and actuation models presented in [Tarokh and McDermott, 2005]. Navigation kinematics is used to monitor rover body rates based on sensed joint motion and is a form of dead-reckoning, whereas slip kinematics is used to estimate the slip and skid rates of a rover's wheels based on sensed joint rates. Actuation kinematics allows a user to define desired actuator or body rates and the undefined driven joint rates are calculated from these. Slip and navigation kinematic models are applied to a simulated wheel-on-leg platform

in [Hidalgo and Cordes, 2012]. A form of actuation kinematics that is based on twist mechanics is presented by [Fu, 2008] and [Alamdari *et al.*, 2013]. This technique provides a solution to the kinematic relationships for a generalised wheel-on-leg platform. It incorporates this model into a motion controller that allows the platform to drive while re-configuring its pose simultaneously.

A tip-over stability model is developed in [Papadopoulos and Rey, 1996] and applied to an actively articulated rover in [Iagnemma *et al.*, 2003]. This model formulates a stability metric based on the kinematic state of the rover and is used as a control input for body reconfiguration so as to ensure stability during traverses over rough terrain.

Demonstrations of operations of real world wheel-on-leg rovers are featured in [Wilcox *et al.*, 2007] with the six-legged ATHLETE rover, while in [Cordes and Kirchner, 2014] the four-legged SHERPA rover is used.

The main contribution of this paper is the derivation of an actuation kinematic model that allows for execution of synchronous motion primitives for a wheel-on-leg platform. Additionally, experimental trials are presented in which the application of the kinematic model along with a static stability monitor ensuring safe rover operations are showcased. The MAMMOTH rover, a wheel-on-leg platform with 16 degrees of actuated freedom is used for the experimental application of the kinematic and stability models. The rover, shown in Figure 1 has four degrees of freedom in each leg, capable of rotating its hips (H), raising and lowering its thighs (Th), steering its wheels (W), and driving its wheels. The positioning of each of these joints is shown in Figure 3.

The article presents the actuation kinematic model in Section 2, followed by the stability model in Section 3. Various rover motions are performed using the MAMMOTH rover platform and analysed in Section 4. Lastly, conclusions and a summary of future works are presented in Section 5.

2 Kinematics

A kinematic model is used to find the resultant wheel and ankle joint velocities that allow for any type of operator defined motion of the MAMMOTH rover on a flat surface. It is assumed that an operator defines the following parameters when tele-operating the rover:

- Driving speed and heading.
- Hip angular velocity and hip position.
- Thigh extension rate and thigh extension position.

This kinematic model takes advantage of the rover's ability to drive in any direction about any instantaneous centre of rotation (ICR) [Campion *et al.*, 1996], pack or unpack, and raise or lower itself. The first step in formulating this model is to develop the forward kinematics of the rover that gives the motion of the rover's body coordinate frame relative to the inertial frame as a function of its joint angular positions and user-defined angular velocities. The next step is to find the wheel and ankle rates required to meet the user-defined body and joint motions. The wheel and ankle rates are found based on a resultant velocity vector for each wheel coordinate frame relative to the associated ankle coordinate frame. The resultant velocity vector represents the combination of user-defined motions at each wheel, allowing for simultaneous driving, packing and raising or lowering of the rover chassis.

2.1 Forward Kinematics

To formulate the forward kinematic relationship between the rover's body and its joints, it is first necessary to assign coordinate frames to each of the joints that affect or are directly affected by the motion of the platform. The rover's coordinate frames are shown in Figures 2 and 3.

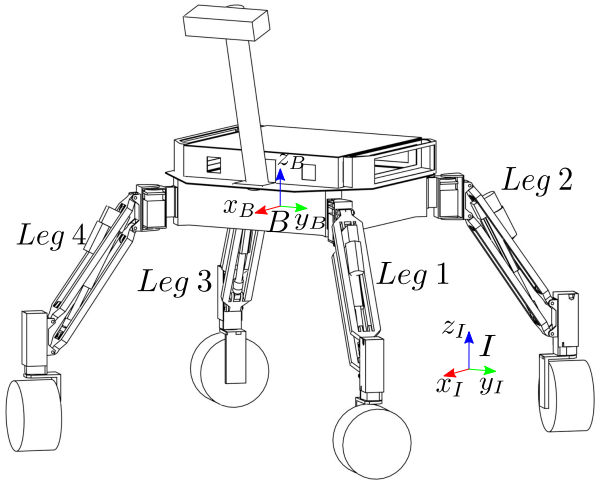

Figure 2: The body and inertial coordinate frames of the MAMMOTH rover along with leg numbers.

Frame I is the inertial coordinate frame. Frame B is the body coordinate frame and it is placed at the centre of the robot's chassis. Frames H_i, U_i, Th_i, Lo_i, A_i and W_i are the hip, upper thigh, thigh, lower thigh, ankle and wheel frames for leg i respectively. The index i denotes the number of the leg within the set of m legs, where $m = 4$ for the MAMMOTH rover.

The MAMMOTH rover moves by actuating sets of its 16 actuators, with four actuators per leg. A sketch of a MAMMOTH leg, its joint coordinate frames and dimensions is shown in Figure 3. Leg i has an angular position, $q_{H,i}$, a prismatic thigh joint stroke position, $q_{Th,i}$, a rotary ankle joint angular position, $q_{A,i}$, and a wheel joint angular position, $q_{W,i}$. The rates at which

each of these joints move are dentoed by their derivatives, such as $\dot{q}_{W,i}$ for the wheel i's angular rate. For the purposes of this work, it is assumed that $\dot{q}_{H,i}$ and $\dot{q}_{Th,i}$ are operator-defined, while $\dot{q}_{A,i}$ and $\dot{q}_{W,i}$ are dependent variables.

To transform coordinates between two coordinate frames, a homogeneous transformation matrix is used. The homogeneous transformation matrix $\mathbf{T}_{JK}$ can be used to transform coordinates from frame K to frame J. The structure of the homogeneous transformation matrix is

$$\mathbf{T}_{JK} = \begin{bmatrix} \mathbf{R}_{JK} & \mathbf{d}_{JK} \\ \mathbf{0} & 1 \end{bmatrix} \tag{1}$$

where $\mathbf{R}_{JK}$ is the rotation matrix from frame K to J and $\mathbf{d}_{JK}$ is the translation vector from K to J.

To find the inverse transformation from coordinate frame K to J, the inverse of Eq. (1) is used:

$$\mathbf{T}_{KJ} = \mathbf{T}_{JK}^{-1}. \tag{2}$$

Homogeneous transformation matrices can be used to form a kinematic chain, which in the case of the MAMMOTH rover is used to develop a relationship between the B and W_i frames. The kinematic chain of a MAMMOTH leg is expressed as:

$$\mathbf{T}_{BW_i} = \mathbf{T}_{BH_i} \cdot \mathbf{T}_{H_iU_i} \cdot \mathbf{T}_{U_iLo_i} \cdot \mathbf{T}_{Lo_iA_i} \cdot \mathbf{T}_{A_iW_i} \tag{3}$$

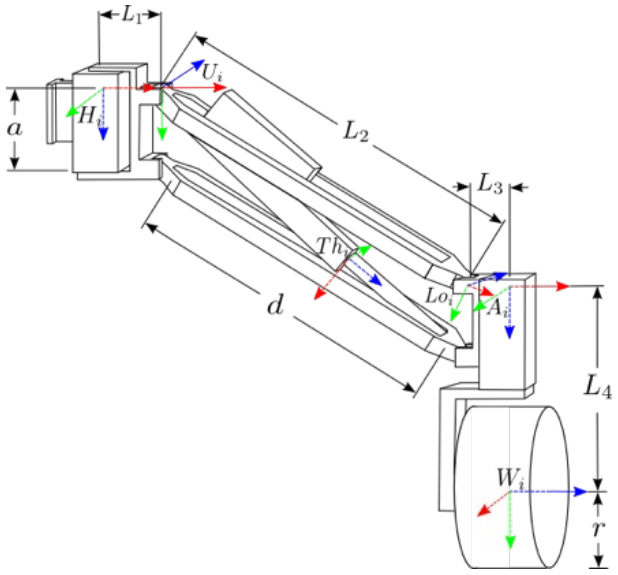

Figure 3: A MAMMOTH rover leg with labeled coordinate frames and dimensions used in the Denavit-Hartenberg representation of the leg's kinematic chain.

The transformation matrix, $\mathbf{T}_{BH_i}$, is a function of the hip angular offset angle κ_i and the hip displacement offset, L_0 as shown in Figure 5. $\mathbf{T}_{BH_i}$ is expressed as:

$$\mathbf{T}_{BH_i} = \begin{bmatrix} \cos\kappa_i & \sin\kappa_i & 0 & L_0\cos\kappa_i \\ \sin\kappa_i & -\cos\kappa_i & 0 & L_0\sin\kappa_i \\ 0 & 0 & -1 & 0 \\ 0 & 0 & 0 & 1 \end{bmatrix}. \tag{4}$$

Table 1: The DH-parameter table for a MAMMOTH leg kinematic chain.

Joint	β	d	α	r
H_i	q_{H_i}	0	$\pi/2$	L_1
U_i	q_{U_i}	0	0	L_2
Lo_i	$-q_{U_i}$	0	$-\pi/2$	L_3
A_i	$q_{A_i}+\pi/2$	L_4	$\pi/2$	0
W_i	q_{W_i}	0	0	0

The chain of transformation matrices from H_i to W_i can be expressed using Denavit-Hartenberg (DH) parameters presented in Table 1. Each row of Table 1 represents a transformation matrix. The general expression for a transformation matrix using DH parameters from frame K to J is:

$$\mathbf{T}_{JK} = \begin{bmatrix} c\beta & -s\beta c\alpha & s\beta s\alpha & rc\beta \\ s\beta & c\beta c\alpha & -c\beta s\alpha & r\sin\beta \\ 0 & s\alpha & c\alpha & d \\ 0 & 0 & 0 & 1 \end{bmatrix} \tag{5}$$

where c and s are used for sin and cos respectively.

2.2 Resultant Wheel Velocities

To determine the necessary wheel and ankle frame velocities, the resultant of wheel frame velocity vectors due to individual primitive rover motions is found. The motion primitives that the MAMMOTH rover is capable of performing include:

1. Driving in any direction about any ICR.
2. Moving its hips so as to pack or unpack its legs.
3. Raising or lowering its body by moving the prismatic linear actuator joints embedded within the legs' parallel thigh linkages.

Each of these motion primitives requires the legs' wheels to be in contact with the surface and to be driven with minimal slippage or skidding, resulting in a desired velocity vector originating from each wheel frame. The velocity vector due to driving for wheel i relative to A_i is denoted as $\mathbf{v}_{W_iA_i,1}$, the vector due to hip motion as $\mathbf{v}_{W_iA_i,2}$ and the vector due to thigh motion as $\mathbf{v}_{W_iA_i,3}$. The magnitude of each of these vectors equals the angular rate of the wheel multiplied by the radius of the

wheel, $\dot{q}_{W_i} r_i$, while the orientation of each vector is the required ankle angle q_{Ai}. Figure 4 shows an example resultant wheel velocity vector and the three wheel vectors that are associated with the possible MAMMOTH rover primitive motions.

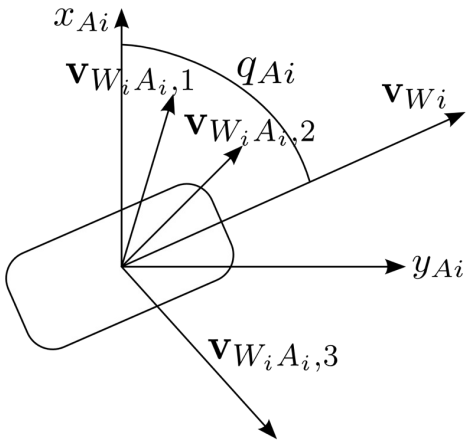

Figure 4: A top view of a MAMMOTH rover wheel, showing an example resultant wheel velocity vector, $\mathbf{v}_{W_i A_i}$, and its components that represent the wheel velocity due to each of the rover's motion primitives.

To find $\mathbf{v}_{W_i A_i,1}$, the ICR, $\mathbf{s}_B$, about which the rover is to drive and the maximum wheel drive speed, $\dot{q}_{W,1,max}$ are taken as inputs from the operator. $\mathbf{s}_B$ is a 3×1 vector that contains the Cartesian coordinates of the ICR relative to the rover's body frame, B as shown in Figure 5. One must then find the desired ankle angle due to wheel driving, $q_{A_i,1}$. To do this, the ICR is expressed in the ith ankle's coordinate frame:

$$\mathbf{s}_{Ai} = \mathbf{R}_{A_i B}\mathbf{s}_B + \mathbf{d}_{A_i B} \tag{6}$$

$q_{A_i,1}$ can then be found as:

$$q_{A_i,1} = \arctan \frac{\mathbf{s}_{A_i,y_{A_i}}}{\mathbf{s}_{A_i,x_{A_i}}} \tag{7}$$

To calculate the magnitude of $\mathbf{v}_{W_i A_i,1}$ the velocity of the wheel frame, W_i due to driving motion needs to be found. This is a function of the user-defined maximum wheel speed due to driving, $\dot{q}_{W,1,max}$, and the distance of W_i from the ICR, $||\mathbf{s}_{W,i}||$. The ICR is expressed relative to W_i by

$$\mathbf{s}_{Wi} = \mathbf{R}_{W_i B}\mathbf{s}_{W_i} + \mathbf{d}_{W_i B} \tag{8}$$

The wheel with the maximum $||\mathbf{s}_{W,i}||$ value is assigned a wheel speed equal to $\dot{q}_{W,1,max}$, and the remaining wheel speeds are calculated relative to this by:

$$||\mathbf{v}_{W_i A_i,1}|| = \dot{q}_{W,1,max} r \,\mathrm{sgn}(\mathbf{s}_{W_i,z_W}) \frac{||\mathbf{s}_{W_i}||}{||\mathbf{s}_{W,max}||}. \tag{9}$$

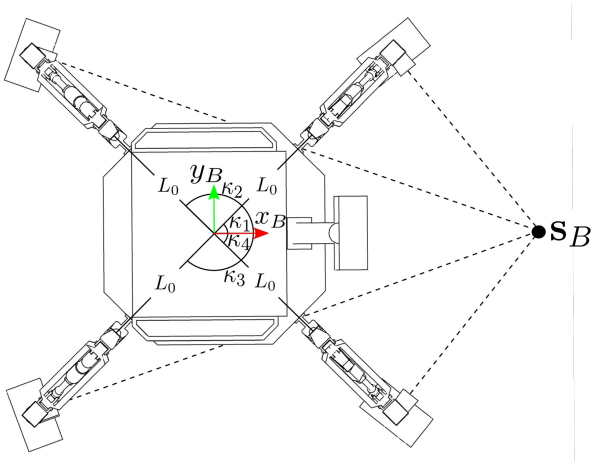

Figure 5: A top view of the MAMMOTH rover with each of its wheels oriented so it can steer about an instantaneous centre of rotation (ICR) in front of the rover. Geometric constants expressing the relationship between the body coordinate frame and each of the leg's hips are also shown.

The velocity vector due the driving motion is then given as:

$$\mathbf{v}_{WiAi,1} = \begin{bmatrix} ||\mathbf{v}_{W_i A_i,1}|| \cos q_{A_i,1} \\ ||\mathbf{v}_{W_i A_i,1}|| \sin q_{A_i,1} \end{bmatrix} \tag{10}$$

The wheel velocity vector due to hip packing, $\mathbf{v}_{W_i A_i,2}$, is found as a function of the user-defined hip rate, $q_{H,i}$.

The magnitude of the wheel velocity vector due to hip motion in the ankle frame can be expressed as:

$$||\mathbf{v}_{WiAi,2}|| = \dot{q}_{H_i}(L_1 + L_2 \cos q_{U_i} + L_3) \tag{11}$$

Given that the motion of W_i due to hip motion only occurs tangentially to the leg, $q_{A_i,2} = 0°$. $\mathbf{v}_{W_i A_i,2}$ is therefore:

$$\mathbf{v}_{W_i A_i,2} = \begin{bmatrix} ||\mathbf{v}_{W_i A_i,2}|| \\ 0 \end{bmatrix} \tag{12}$$

The velocity vector due to thigh motion can be expressed as:

$$||\mathbf{v}_{W_i,3}|| = \frac{\dot{q}_U L_2 \sin q_U}{r}. \tag{13}$$

$\dot{q}_{U_i}$ a function of the operator defined linear actuator rate, $\dot{q}_{Th_i}$ and the current thigh angle, q_{U_i}:

$$\dot{q}_{U_i} = \frac{\dot{q}_{Th_i}}{ad\sin(\pi/2 + q_{U_i})\left(a^2 + d^2 - 2ad\cos(\pi/2 + q_{U_i})\right)^{1/2}} \tag{14}$$

where a and d are geometric constants shown in Figure 3.

Given that the motion of W_i due to thigh motion only occurs longitudinally along the leg, $q_{Ai,2} = \pi/2$. The velocity vector due to thigh actuation can therefore be expressed as:

$$\mathbf{v}_{W_iA_i,3} = \begin{bmatrix} 0 \\ ||\mathbf{v}_{W_iA_i,3}|| \end{bmatrix} \tag{15}$$

Lastly, the resultant wheel velocity vector is found as the sum of the three component velocity vectors from Eqs. (10), (12) and (15):

$$\mathbf{v}_{Wi} = \begin{bmatrix} r\dot{q}_{W_i,1,max}\,\mathrm{sgn}(\mathbf{s}_{W_i,z_W})\frac{||\mathbf{s}_{W_i}||}{||\mathbf{s}_{W_{max}}||}\cos\left(\arctan\frac{\mathbf{s}_{A_i}(2)}{\mathbf{s}_{A_i}(1)}\right)... \\ +\dot{q}_{H_i}(L_1 + L_2\cos q_{U_i} + L_3) \\ r\dot{q}_{W,1,max}\,\mathrm{sgn}(\mathbf{s}_{W_i,z_W})\frac{||\mathbf{s}_{W_i}||}{||\mathbf{s}_{W_{max}}||}\sin\left(\arctan\frac{\mathbf{s}_{A_i}(2)}{\mathbf{s}_{A_i}(1)}\right)... \\ +\frac{\dot{q}_{Th_i}L_2\sin q_{U_i}}{rad\sin(\pi/2+q_{U_i})\left(a^2+d^2-2ad\cos(\pi/2+q_{U_i})\right)^{1/2}} \end{bmatrix}. \tag{16}$$

Expressions for the desired $\dot{q}_{W_i}$ and q_{A_i} values can then be found from Eq. (16) as:

$$\dot{q}_{W_i} = \frac{||\mathbf{v}_{W_i}||}{r} \tag{17}$$

$$q_{A_i} = \arctan\frac{\mathbf{v}_{W_i,x_{A_i}}}{\mathbf{v}_{W_i,y_{A_i}}}. \tag{18}$$

With these values it is now possible to command the MAMMOTH rover to move using one or all of its motion primitives simultaneously.

3 Tip-Over Stability

To monitor the stability of the MAMMOTH rover during operations and to alert the operator if they are putting the rover into an unstable configuration a facility for estimating the rover's current stability is required. Given that the MAMMOTH rover is intended to operate at relatively slow speeds, a static tip-over stability model originally formulated by [Papadopoulos and Rey, 1996] is used. This model is based on the stability polygon formed by the rover's wheel ground contact points. If the weight vector extending from the rover's centre of mass intersects with the plane formed by the stability polygon, within the boundaries of the polygon's sides, the rover is assumed to be in a stable state. Figure 6 shows the stability polygon formed when four wheels are in contact with the ground.

The stability estimate, β, in any given kinematic state is a function of η_i, the angle between the weight vector, $\mathbf{f}_g$ extending from the rover's centre of mass and the vector $\mathbf{l}_i$. It is assumed that the centre of mass of the rover

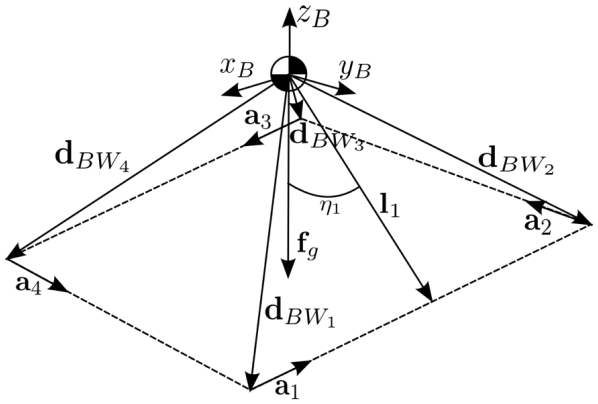

Figure 6: An example stability polygon of the MAMMOTH rover when four wheels are touching the ground.

is approximately equal to the location of the body coordinate frame B. The minimum of the stability angles gives a metric describing how stable the rover is. The vector $\mathbf{l}_i$ is a function of the wheel/ground contact point for leg i and $i+1$. The wheel ground contact point is expressed in the body frame by $\mathbf{d}_{BWi}$, which is the displacement vector of the homogeneous transformation matrix between B and W_i. The vectors connecting the wheel/ground contact points, $\mathbf{a}_i$, are expressed by

$$\mathbf{a}_i = \mathbf{d}_{BWi+1} - \mathbf{d}_{BWi}, \quad i = \{1, ..., m-1\} \tag{19}$$

$$\mathbf{a}_m = \mathbf{d}_{BW1} - \mathbf{d}_{BWm}, \quad i = \{m\}. \tag{20}$$

The vector $\mathbf{l}_i$ originates at B and is orthogonal to $\mathbf{a}_i$. It is expressed as:

$$\mathbf{l}_i = \left(\mathbf{I} - \hat{\mathbf{a}}_i\hat{\mathbf{a}}_i^T\right)\mathbf{d}_{BWi}. \tag{21}$$

A stability angle, η_i is then found from

$$\eta_i = \sigma\arccos\left(\hat{\mathbf{f}}_g \cdot \hat{\mathbf{l}}_i\right), \tag{22}$$

where

$$\sigma = \begin{cases} +1 & \left(\hat{\mathbf{l}}_i \times \hat{\mathbf{f}}_g\right)\cdot\hat{\mathbf{a}}_i > 0 \\ -1 & \text{otherwise} \end{cases} \tag{23}$$

which leads to an expression for the the stability metric

$$\beta = \min\eta_i, \quad i = 1, ..., m. \tag{24}$$

This stability metric indicates an unstable state when it is less than zero. For typical operations, the operator is given the stability metric, β and each of the stability angles η_i as feedback on the current stability state of the rover.

4 Experimental Results

The following experiments are used to demonstrate the various mobility mode's that the MAMMOTH rover is capable of operating in. In doing so, the application of the kinematic model of the rover from Section 2 is showcased. Additionally, the experiments highlight estimates of the kinetostatic stability of the platform during operations according to the stability model from Section 3. Lastly, the performance of the rover in driving along a pre-defined path while using multiple primitive motions synchronously as compared to using a single driving motion primitive is evaluated.

4.1 Setup

The MAMMOTH rover has an 85 kg mass, is powered by 12×95 Wh rechargeable Li-Ion cells. Each of MAMMOTH's rotary joints are actuated by identical 100 W smart actuator units, each containing a DC motor, motor controller and harmonic gear head. The rotary actuators have a maximum continuous operation torque of 24.8 Nm. The rotary actuators are each equipped with a 1000 pulse incremental encoder before gear reduction and a 4096 step absolute encoder after gear reduction. Each of the hip actuators are capable of rotating the hips joints between $q_{Hi} = -135°$ and $q_{Ui} = 135°$, while each of the ankle actuators are capable of rotating the ankle joints between $q_{Ai} = -180°$ and $q_{Ai} = 180°$. The wheel actuators have continuous rotation. The four linear actuators embedded in each of the thighs are capable of applying up to 1500 N and have a 110 mm stroke length, allowing for a thigh angular range between $q_{Ui} = -20°$ and $q_{Ui} = 70°$. The linear actuators each use a potentiometer for position feedback. An inertial measurement unit located within the MAMMOTH rover chassis returns body roll, pitch and yaw data. For the experiments described below, a 1GHz ARM Cortex-A8 Linux computer on board the rover was used to receive actuator drive instructions from a ground control station and send actuator and platform sensor data to the ground control station.

Five motion experiments were performed along a common path to allow for comparison between each experiment. Each experiment was run twice, the results presented are in this section are representative examples of each experiment. The path followed in each experiment is shown in Figure 7. When the rover reaches a target on the path, the rover is reliant on the operator to identify that it has reached the target and for a new driving instruction. The rover starts at target 1 with a heading of 0°, it then drives straight ahead about the ICR, $\mathbf{s_B} = \begin{bmatrix} 0 & \infty \end{bmatrix}$, keeping a constant heading as it moves towards target 2. Upon reaching target 2 the rover drives directly to the side about the ICR, $\mathbf{s_B} = \begin{bmatrix} \infty & 0 \end{bmatrix}$, keeping a constant heading as it moves towards target 3. At target 3, the rover begins to drive back towards target 1 by turning about an ICR, $\mathbf{s}_B = \begin{bmatrix} 0 & -2 \end{bmatrix}$, which is approximately located at target 4. Lastly, upon reaching target 1, the rover performs a spot turn in an anticlockwise direction until it's heading is once again at 0°. In each experiment the rover follows this path while performing distinct manoeuvres. The manoeuvres and numbering of each experiment are as follows:

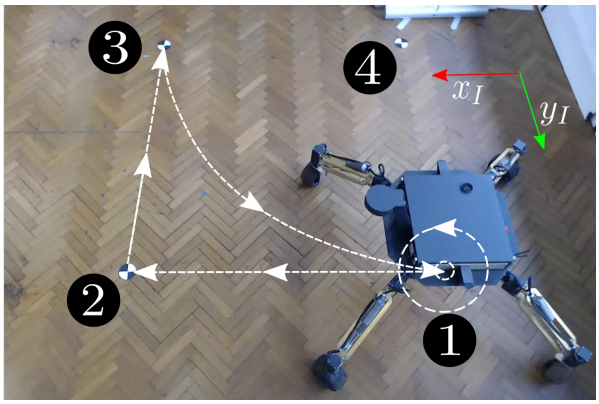

Figure 7: The path followed by the MAMMOTH rover in each experiment with the four labelled targets and inertial coordinate frame.

1. Driving with all hips held at $q_{H_i} = 0°$ and all thighs held at $q_{Thi} = 80$ mm.
2. Driving with all thighs held at $q_{Th_i} = 70$ mm, while packing and unpacking the hips between $q_{H_i} = 130°$ and $q_{H_i} = -130°$.
3. Driving with all hips held at $q_{H_i} = 0°$, while raising and lowering the thighs between $q_{Th_i} = 10$ mm and $q_{Th_i} = 95$ mm.
4. Driving with all hips packing and unpacking between between $q_{Hi} = 130°$ and $q_{H_i} = -90°$ and all thighs raising and lowering between $q_{Th_i} = 10$ mm to $q_{Th_i} = 95$ mm.
5. Driving on three wheels with leg 4 raised to $q_{Th_i} = 0$ mm and the remaining legs at $q_{Th_i} = 50$ mm, with all hips at $q_{H_i} = 0°$.

4.2 Analysis

The sequence of motions performed in each experiment can be seen from the snapshots in Table 2. The table's rows each show an individual experiment, while each column shows the rover at various steps in the path followed. Each experiment step shows the rover while it is executing a motion between path targets. Step 1 shows the rover moving from target 1 to 2, step 2 shows driving between targets 2 to 3, step 3 shows the ICR turn from targets 3 to 1 and step 4 shows the spot turn about target 1.

Table 2: *Snapshots of the MAMMOTH rover between targets. Each row showing an individual experiment. The columns show driving steps, where step 1 is driving straight between targets 1 and 2, step 2 is driving to the side between targets 2 and 3, step 3 is between targets 3 and 1 driving along a curved path centred at target 4, while step 4 is spot turning at target 1. Ghost images of the rover are shown of the rover at the previous step for reference.*

Exp	**Step 1**	**Step 2**	**Step 3**	**Step 4**
1				
2				
3	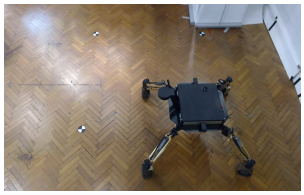			
4			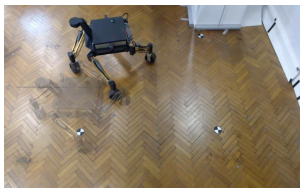	
5		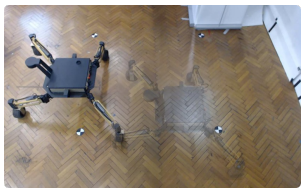	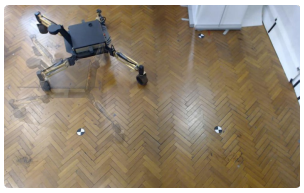	

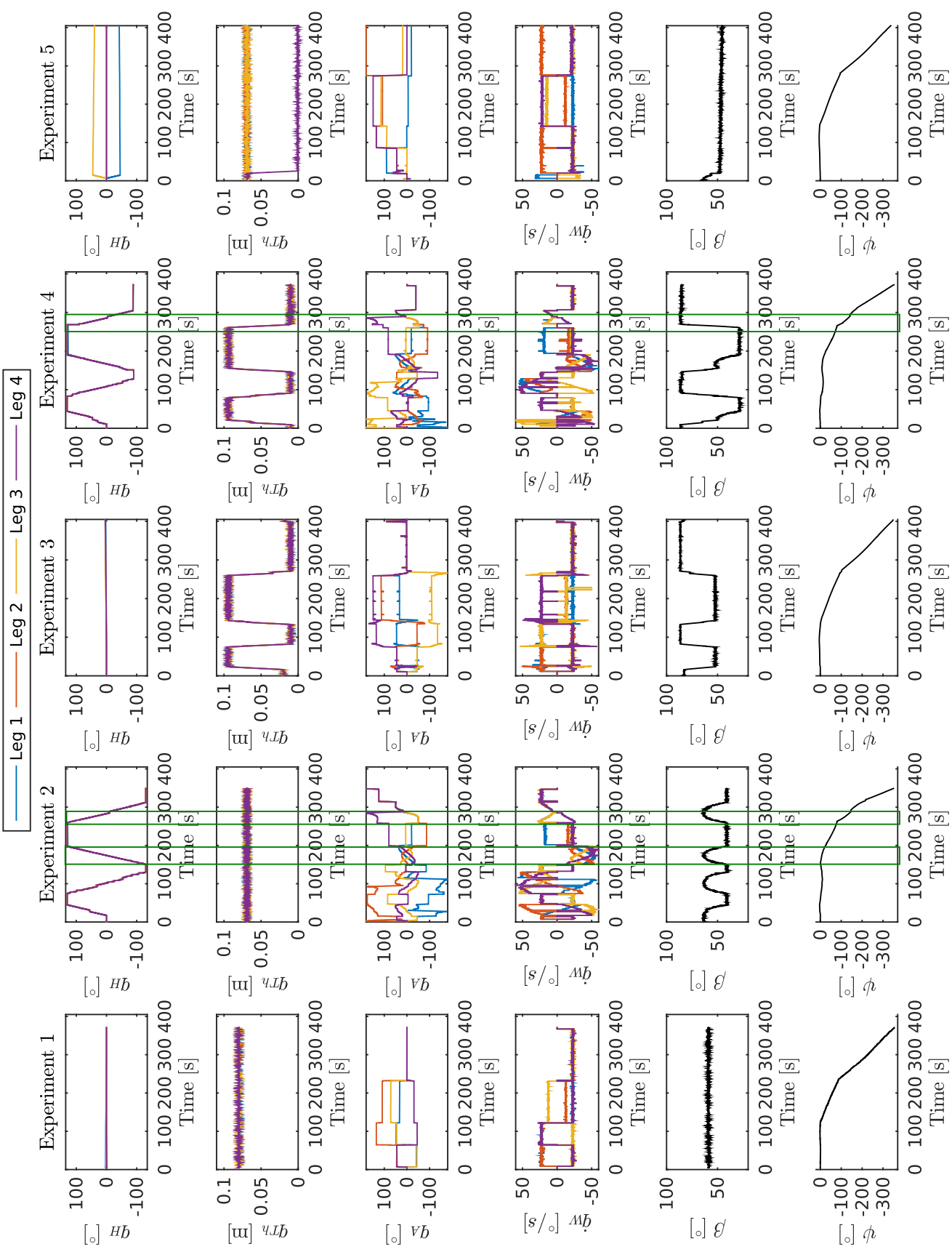

Figure 8: Data collected from each of the five experiments. The hip angles, q_H, thigh stroke positions, q_{Th}, ankle angles, q_A, and wheel rotational rates, q_W, are presented for each leg. Additionally, the stability estimate, β, and the heading, ψ, are shown for each experiment. The green boxes highlight areas specific data ranges of interest, as discussed in Section 4.2

Figure 8 presents data collected from actuator encoders, stability estimates, β, and the heading angle, ψ of the rover for each of the experiments. The hip and and thigh positions match the desired motions given that they are based on operator defined inputs to the system. From observing the ankle position and wheel speed plots it observed that they are dependent on the behaviour of the thigh and hip angular positions. This is quite noticeable when looking at the q_A plot for Experiment 2 between $t = 150$ s to $t = 197$ s, where there is a symmetric angular profile between the four ankle angles while the hip angles are changing. This time range is highlighted by a green box over the Experiment 2 plots in Figure 8. The wheel speed in the $\dot{q}_W$ plot for the same experiment during the same time period also exhibits a symmetric profile between the four legs. At various points in the experiments where simultaneous motions were used, it is observed that the wheel rate goes to $0°/s$ for brief periods of time. This is attributed to the associated ankle driving to an ankle actuator angle equal to or greater than 45°. This angle limit has been chosen to limit the mechanical stresses imposed on the ankle joint.

Based on each experiment having the same desired heading as a function of the global position of the platform, the heading is a metric for defining how well synchronous movements were performed. Figure 8 shows the rover's heading angle as a function of experiment time for each of the experiments in the bottom row of plots. In an ideal case, each of the heading versus time data sets should be the same, being 0° from target 1 to 3, change linearly between 0° and −90° between targets 2 and 3 and then change linearly between −90° and −360° as the spot turn about target 1 is performed.

For each of the experiments, the heading plots follow the same trend. Discrepancies between heading plots are due to multiple items not captured in the kinematic model. A velocity limit of 60°/s was placed on each ankle actuator to ensure safety of the ankle's mechanical joint. In some situations this resulted in a lag in ankle angle and the wheel being driven in a slightly incorrect direction and in turn wheel slippage. Additionally, it is assumed by the kinematic model that the wheel has a contact point with the ground at any point in time. The wheel actually has a contact ellipse. This contact over a surface area results in wheel slippage and sheer stress on the wheel, especially during signifcant changes in ankle angular position while the wheel is being driven. This effect may be noticed in each of the experiment plots from experiment 2 between times $t = 271$ s and $t = 295$ s and in experiment 4 between $t = 272$ s and $t = 300$ s. These time ranges are highlighted by green boxes in Figure 8.

The stability estimate for each experiment is shown in the second last row of Figure 8. Obviously, given that the rover stayed stable throughout all of the experiments, the stability estimates, β, were always greater than 0. The stability of the platform changes whenever the footprint of the rover changes. This is particularly noticeable in experiments 2-4. In experiment 2, the stability angles follow a hyperbolic path as the hip angles change at a constant rate. In this experiment the platform is at its least stable when its legs are in their fully "packed" state when $q_H = 130°$. In experiment 3, the stability angles are also seen to change as the body is raised and lowered and the contact points get closer and further away from the body respectively. From all of the experiments performed, the platform adopts its most stable configuration when it is closest to the ground plane, with the hips at $q_H = 0°$ as seen in experiments 3 and 4. The most unstable configuration is observed in experiment 4 when the hips are in their packed configuration and the body is raised high above the ground.

5 Conclusions and Future Work

Synchronous execution of primitive mobility modes have been described using a wheel vector kinematic method and have been validated in motion control of the MAMMOTH rover. Additionally, a static stability monitoring technique is described and demonstrated. These capabilities allow for tele-operation of the MAMMOTH rover on a planar surface.

The experimental results presented demonstrate that the kinematic model of the rover's motions is adequate, however does suffer from disturbances to desired heading, especially when multiple primitive motions are superimposed on each other. To address this, future work will focus on implementing a body motion feedback controller that adjusts joint motions to reduce the effect of external perturbations.

Given the validation of the presented kinematic model, an extension of this model to a non-planar surface will be considered for operations on rough terrain. In addition, the existing kinematic model will be extended to include motion primitives needed to form clambering gaits for overcoming significant obstacles that cannot be traversed by wheel driving alone.

Acknowledgments

We would like to acknowledge the Australian Government's Broadband Enabled Education and Skills Services Programme, which funded The Mars Lab project. The project is the result of a partnership between the University of Sydney, the University of New South Wales, and the Powerhouse Museum, Sydney. We would also like to thank Muhammad Esa Attia, Javier Martinez, Dewey Nguyen, Steven Potiris, Iwan Kelaiah, Thomas Teo and Benjamin Stewart for all of their help

in the design, build, operation and maintenance of the MAMMOTH rover.

References

[Alamdari *et al.*, 2013] Aliakbar Alamdari, Xiaobo Zhou, and Venkat Krovi. Kinematic Modeling, Analysis and Control of Highly Reconfigurable Articulated Wheeled Vehicles. In *Proceedings of the ASME 2013 International Design Engineering Technical Conference & Computers and Information in Engineering Conference IDETC/CIE*, pages 1–7, Portland, 2013.

[Campion *et al.*, 1996] Guy Campion, Georges Bastin, and Brigitte D Andrca-novel. Structural Properties and Classification of Kinematic and Dynamic Models of Wheeled Mobile Robots. *IEEE Transactions on Robotics and Automation*, 12(1):47–62, 1996.

[Cordes and Kirchner, 2014] Florian Cordes and Frank Kirchner. Reconfigurable Integrated Multirobot Exploration System (RIMRES): Heterogeneous Modular Reconfigurable Robots for Space Exploration. *Journal of Field Robotics*, 31(1):3–34, 2014.

[Fu, 2008] Qiushi Fu. Kinematics of Articulated Wheeled Robots: Exploiting Reconfigurability and Redundancy. Master's thesis, State University of New York at Buffalo, 2008.

[Hidalgo and Cordes, 2012] Javier Hidalgo and Florian Cordes. Kinematics Modeling of a Hybrid Wheeled-Leg Planetary Rover. In *International Symposium on Artificial Intelligence, Robotics and Automation in Space*, Turin, 2012.

[Iagnemma *et al.*, 2003] Karl Iagnemma, Adam Rzepniewski, and Steven Dubowsky. Control of Robotic Vehicles with Actively Articulated Suspensions in Rough Terrain. *Autonomous Robots*, 14:5–16, 2003.

[Papadopoulos and Rey, 1996] E G Papadopoulos and D A Rey. A New Measure of Tipover Stability Margin for Mobile Manipulators. In *Proceedings of the 1996 IEEE International Conference of Robotics and Automation*, pages 3111–3116, Minneapolis, April 1996.

[Tarokh and McDermott, 2005] M. Tarokh and G.J. McDermott. Kinematics Modeling and Analyses of Articulated Rovers. *IEEE Transactions on Robotics*, 21(4):539–553, August 2005.

[Wilcox *et al.*, 2007] B Wilcox, T Litwin, J Besiadecki, J Matthews, M Heverly, J Morrison, J Townsend, N Ahmad, a Sirota, and B Cooper. ATHLETE: A Cargo Handling and Manipulation Robot for the Moon. *Journal of Field Robotics*, 24(5):421–434, 2007.